



Cite this: *J. Mater. Chem. A*, 2024, **12**, 16921

Retarded O₂ transport in Co²⁺-coordinated supramolecular polymer networks for membrane CO₂/O₂ separations†

Taliehsadat Alebrahim, Narjes Esmaeili, Gengyi Zhang and Haiqing Lin  *

Dissociated Co²⁺ ions in liquids and polymers have been demonstrated to reversibly react with O₂ and increase O₂ permeability. However, we find a series of Co²⁺-coordinated supramolecular polymer networks (SPNs) with enormous O₂ sorption but retarded diffusion, leading to superior CO₂/O₂ separation properties. Specifically, Co(BF₄)₂ is dissolved by cross-linked poly(ethylene oxide) (XLPEO), as validated by Fourier transform infrared (FTIR) spectroscopy, X-ray diffraction (XRD), and differential scanning calorimetry (DSC). The dissociated Co²⁺ ions increase O₂/CO₂ solubility selectivity but decrease its diffusivity selectivity. For example, adding 6.4 mass% Co(BF₄)₂ in XLPEO increases O₂ solubility by 35 times and O₂/CO₂ solubility selectivity from 0.12 to 5.0, but it decreases O₂/CO₂ diffusivity selectivity from 0.40 to 0.0058, leading to a CO₂/O₂ permeability selectivity of 35, above Robeson's upper bound and superior to that of state-of-the-art polymers. This study unravels an exciting platform of metal ion-coordinated supramolecular networks for various molecular separations by harnessing strong affinity but retarded diffusion despite their stability challenge.

Received 7th April 2024
Accepted 3rd June 2024

DOI: 10.1039/d4ta02376e
rsc.li/materials-a

Introduction

CO₂/O₂ separations are of great interest for healthcare and industrial applications. For instance, artificial lungs for CO₂ and O₂ exchange are critical for blood oxygenation;^{1,2} atmospheric CO₂ and O₂ compositions can be manipulated for storing and transporting vegetables and fruit to improve their shelf lifetime;³ CO₂ capture from fossil fuel-derived flue gas has been proposed as a critical way to mitigate CO₂ emissions to the atmosphere, and the flue gas contains 4–16% O₂ that needs to be separated from CO₂.^{4,5} Membrane technology offers a cost- and energy-efficient approach for gas separations. However, CO₂ has a kinetic diameter of 3.3 Å, very close to that of O₂ (3.46 Å), and therefore, most polymers do not have sufficiently strong size-sieving ability to obtain high diffusivity selectivity and thus permeability selectivity. For example, Matrimid is widely investigated for membrane separations due to its strong size-sieving ability, and it showed a CO₂/CH₄ selectivity of 35 but a CO₂/O₂ selectivity of only 3.8 at 35 °C.⁶

Gas separation properties can be often manipulated through interactions between polymers and targeted gases. For example, polymers containing poly(ethylene oxide) (PEO) demonstrate good CO₂/O₂ separation properties because of their affinity towards CO₂, leading to excellent CO₂/O₂ solubility selectivity.^{7–9}

PEO exhibited a CO₂/O₂ selectivity of 18, though its CO₂/CH₄ selectivity was only 20,⁸ much lower than that of Matrimid.

Co²⁺ forms complexes with O₂, leading to high O₂ sorption, and thus, Co²⁺-based O₂-binding carriers have been reported, such as cobalt porphyrins,¹⁰ cobalt(II) complexes,¹¹ cobalt(II)-based metal-containing ionic liquid (MCIL),^{12,13} and Co-based metal-organic frameworks (MOFs).¹⁴ These carriers were incorporated into liquid membranes to improve O₂/gas separation performance,^{12,15,16} as shown in Table 1. For example, introducing Co (3-MeOsaltmen) in dimethylacetamide (DMAc) increased O₂/N₂ selectivity from 1.9 to 25 and achieved O₂ permeability as high as 270 barrer (1 barrer = 10⁻¹⁰ cm³(STP) cm cm⁻² s⁻¹ cm_{Hg}⁻¹).¹¹ However, liquid membranes face instability challenges because of solvent evaporation, pressure-induced liquid loss, and carrier activity loss.

To overcome the instability of liquid membranes, Co²⁺-based carriers were dissolved in solid polymers by ion coordination to form supramolecular polymer networks (SPNs) with good mechanical properties.^{20–22} The dissociated Co²⁺ can reversibly bind O₂, improving O₂/N₂ separation properties (Table 1). For instance, adding 1 wt% cobalt(II) phthalocyanine (CoPc) in Pebax 1657 (a microphase-separated block copolymer containing PEO and nylon) increased O₂/N₂ selectivity from 2.9 to 8.5.¹⁶ Similar approaches have been adopted to develop Ag⁺-coordinated SPNs for olefin/paraffin separations. As Ag⁺ forms complexes with olefins, AgBF₄ was dissolved in Pebax to dramatically increase ethylene/ethane selectivity from 1 to 30.^{23,24}

In striking contrast, we report retarded O₂ transport in the SPNs prepared from Co(BF₄)₂ dissolved in crosslinked PEO

Department of Chemical and Biological Engineering, University at Buffalo, The State University at New York, Buffalo, New York 14260, USA. E-mail: haiqingl@buffalo.edu

† Electronic supplementary information (ESI) available. See DOI: <https://doi.org/10.1039/d4ta02376e>



Table 1 Enhanced O₂ transport properties in conventional liquid membranes and polymers containing Co²⁺-based carriers

Facilitated transport membranes

| Polymers/liquids | Cobalt carriers | Carrier content (wt%) | Temp. (°C) | Pressure (bar) | O ₂ permeability (barrer) | O ₂ /N ₂ selectivity |
|-----------------------------|--|-----------------------|------------|----------------|--------------------------------------|--|
| DMAc ¹¹ | Co (3-MeOsaltmen) | 15 | -10 | 0.19 | 270 | 25 |
| Pebax 1657 (ref. 16) | CoPc | 1 | 25 | 2 | 224 | 8.5 |
| Polycarbonate ¹⁷ | CoSalen | 3 | 5 | 3 | 0.33 | 15 |
| PDMS ¹⁸ | CoSalen | 20 | 30 | 0.05 | 46 ^a | 7.7 |
| PIM-1 (ref. 19) | mim ₂ Co (NCS) ₄ | 2.0 | 30 | 2 | 113 | 5.3 |

^a GPU, 1 GPU = 10⁻⁶ cm³(STP) cm⁻² s⁻¹ cm_{Hg}⁻¹.

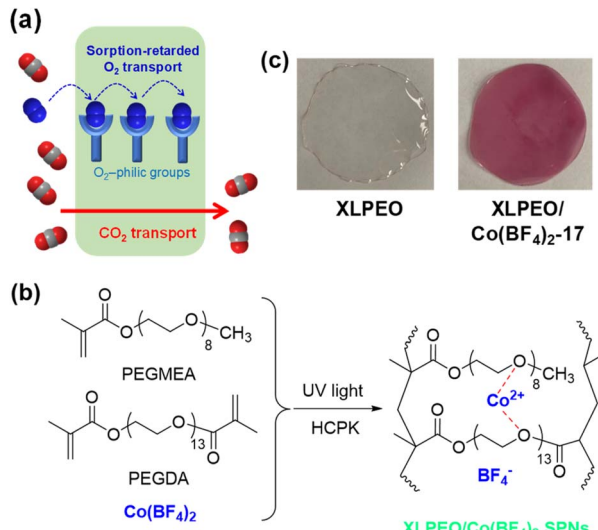


Fig. 1 Co²⁺-coordinated SPNs with superior CO₂/O₂ separation properties. (a) Schematic of O₂-retarded transport facilitating CO₂/O₂ separation. (b) Schematic of XLPEO prepared from PEGDA and PEGMEA and its interactions with Co(BF₄)₂. (c) Photos of XLPEO/salt-x films.

(XLPEO) synthesized from poly(ethylene glycol) methyl ether acrylate (PEGMEA) and poly(ethylene glycol) diacrylate (PEGDA) (Fig. 1). The Co ions complex with ether oxygens, enabling complete dissociation of the Co salts, as evidenced by transparent and uniform films obtained (Fig. 1c), leading to extremely high O₂ sorption. However, instead of improving O₂ permeability, increasing the Co(BF₄)₂ content in XLPEO dramatically decreases O₂ permeability and increases CO₂/O₂ selectivity. The effect of Co ions on the structures and CO₂/O₂ transport properties of the SPNs is thoroughly investigated to derive structure and property relationships. This study unveils a new mechanism for harnessing strong binding capabilities with a penetrant to lower its diffusivity and permeability and enable its separation from other penetrants.

Experimental

Materials

PEGDA ($n = 13$; $M_n = 700$ g mol⁻¹), PEGMEA ($n = 9$; $M_n = 480$ g mol⁻¹), 1-hydroxycyclohexyl phenyl ketone (HCPK), and Co(ClO₄)₂·6H₂O were received from Sigma Aldrich Corporation

(St. Louis, MO). Co(BF₄)₂·6H₂O was purchased from Thermo Fisher Scientific (Waltham, MA). Gas cylinders of O₂, N₂, and CO₂ (99.99%) were obtained from Airgas Inc. (Buffalo, NY).

Preparation of Co²⁺-coordinated SPNs

To prepare SPNs, PEGDA, PEGMEA, HCPK (0.1 mass% relative to PEGDA and PEGMEA), and Co salt were dissolved in water. The mass ratio of PEGDA to PEGMEA was set at 1 : 4 to obtain XLPEO with high gas permeability and good mechanical properties.²⁵ The prepolymer solution was sandwiched between two quartz plates and photopolymerized using UV light with a wavelength of 254 nm at 3.0 mW cm⁻² for 5 min.²⁶ The obtained solid films were vacuumed at ≈ 23 °C for three days or more to remove water and then kept under vacuum before use. The samples are named XLPEO/salt-x, where x represents the mass% of the salt in the dried films.

Characterization of SPNs

Film thickness was measured using a digital micrometer (Mitutoyo Corporation, Kanagawa, JP). An attenuated total reflection-Fourier transform infrared (ATR-FTIR) spectrometer (Vertex 70, Billerica, MA) was utilized at a resolution of 4 cm⁻¹ to investigate the conversion of PEGDA and PEGMEA and the salt state in XLPEO. The SPN structure was examined using an Ultima IV X-ray diffractometer (XRD, Rigaku Corporation, Tokyo, JP) with CuK α radiation (a wavelength of 1.54 Å) at ≈ 23 °C. Thermal transitions were obtained by Differential Scanning Calorimetry (DSC, Q2000, TA Instruments, New Castle, DE). Two heating cycles were carried out from -90 to 100 °C at 10 °C min⁻¹ in a N₂ atmosphere. Glass transition temperature (T_g) was determined as the inflection point of a step change in the second heating cycle. SPN density, ρ_{SP} (g cm⁻³), was determined using an analytical balance equipped with a density kit.^{26,27}

Pure-gas permeability of the SPN films was determined using a constant-volume and variable-pressure apparatus at different feed pressures (4.4, 7.9, and 11.3 bar) and 35 °C.²⁸ The measurement followed an order of N₂, CO₂, and O₂. N₂ was also re-tested for some samples after O₂ to ensure that the samples remained intact after O₂ exposure. Gas permeability has an uncertainty of less than 10%, estimated using an error propagation analysis.²⁹ Pure-gas sorption in the SPNs (~ 2 g) was determined using a dual-volume and dual-transducer apparatus



based on the pressure-decay method at 35 °C and three pressures (~ 4.5 , ~ 7.9 , and ~ 11.4 bar).³⁰

Results and discussion

Physical and chemical properties of Co^{2+} -coordinated SPNs

Fig. 2a exhibits FTIR spectra of XLPEO/Co(BF₄)₂ SPNs. The peak at 1096 cm⁻¹ representing C–O vibration in XLPEO redshifts with increasing Co(BF₄)₂ content, indicating the weakened C–O

bonds caused by the interactions with Co^{2+} .^{26,31} For example, adding 17 mass% Co(BF₄)₂ lowers the C–O stretching frequency from 1097 to 1057 cm⁻¹. By contrast, increasing the Co(BF₄)₂ content has minimal impact on the C=O stretching at 1732 cm⁻¹, indicating the absence of strong interactions with Co^{2+} . Similar behaviors have been observed for XLPEO/Co(Cl₄)₂ (Fig. S1a†). Additionally, the SPNs exhibit a new peak at 623 cm⁻¹ characteristic of free ClO₄⁻ anions, confirming the dissociation of Co(ClO₄)₂ by XLPEO.³¹

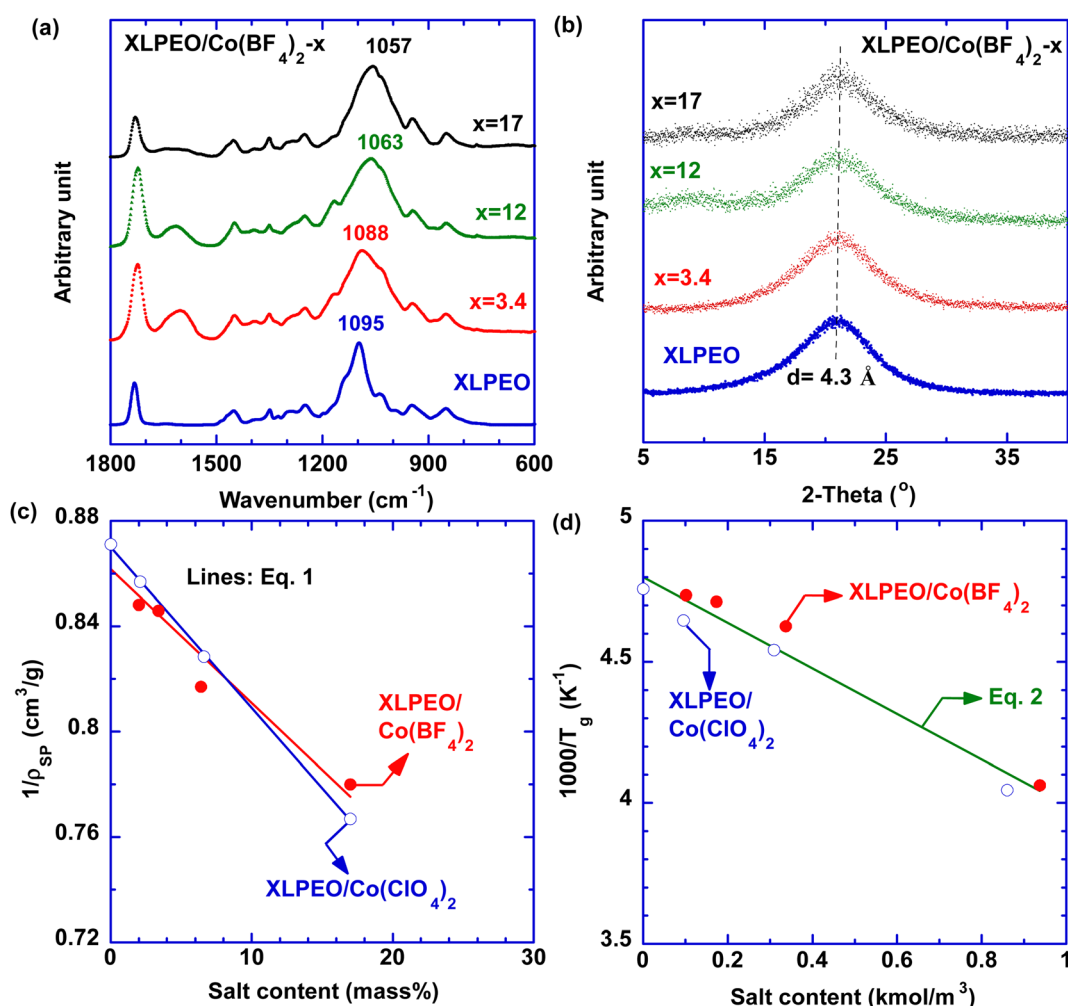


Fig. 2 Physical properties of SPNs. (a) FTIR spectra and (b) XRD patterns of XLPEO/Co(BF₄)₂. (c) Correlation between ρ_{SP} and the salt content using eqn (1). (d) Correlation between T_g and the salt content using eqn (2).

Table 2 Physical properties of XLPEO/Co(BF₄)₂-x including r (molar ratio of ether oxygens to Co^{2+} ions), ρ_{SP} , $T_{g,\text{SP}}$, and pure-gas permeability and selectivity at 35 °C

| x (mass%) | r | ρ_{SP} (g cm ⁻³) | $T_{g,\text{SP}}$ (°C) | P_A (barrer) | | | Selectivity | | |
|----------------|-----|--|------------------------|----------------|----------------|-----------------|---------------------------------|---------------------------------|--------------------------------|
| | | | | N ₂ | O ₂ | CO ₂ | CO ₂ /N ₂ | CO ₂ /O ₂ | O ₂ /N ₂ |
| 0 | — | 1.149 | -63 | 10 | 26 | 510 | 51 | 20 | 2.6 |
| 2 | 259 | 1.179 | -63 | 2.9 | 2.2 | 109 | 38 | 50 | 0.76 |
| 3.4 | 150 | 1.182 | -62 | 1.2 | 0.82 | 33 | 28 | 40 | 0.68 |
| 6.4 | 77 | 1.224 | -57 | 0.49 | 0.40 | 15 | 31 | 38 | 0.82 |
| 17 | 26 | 1.282 | -27 | 0.24 | 0.14 | 8.4 | 35 | 60 | 0.58 |

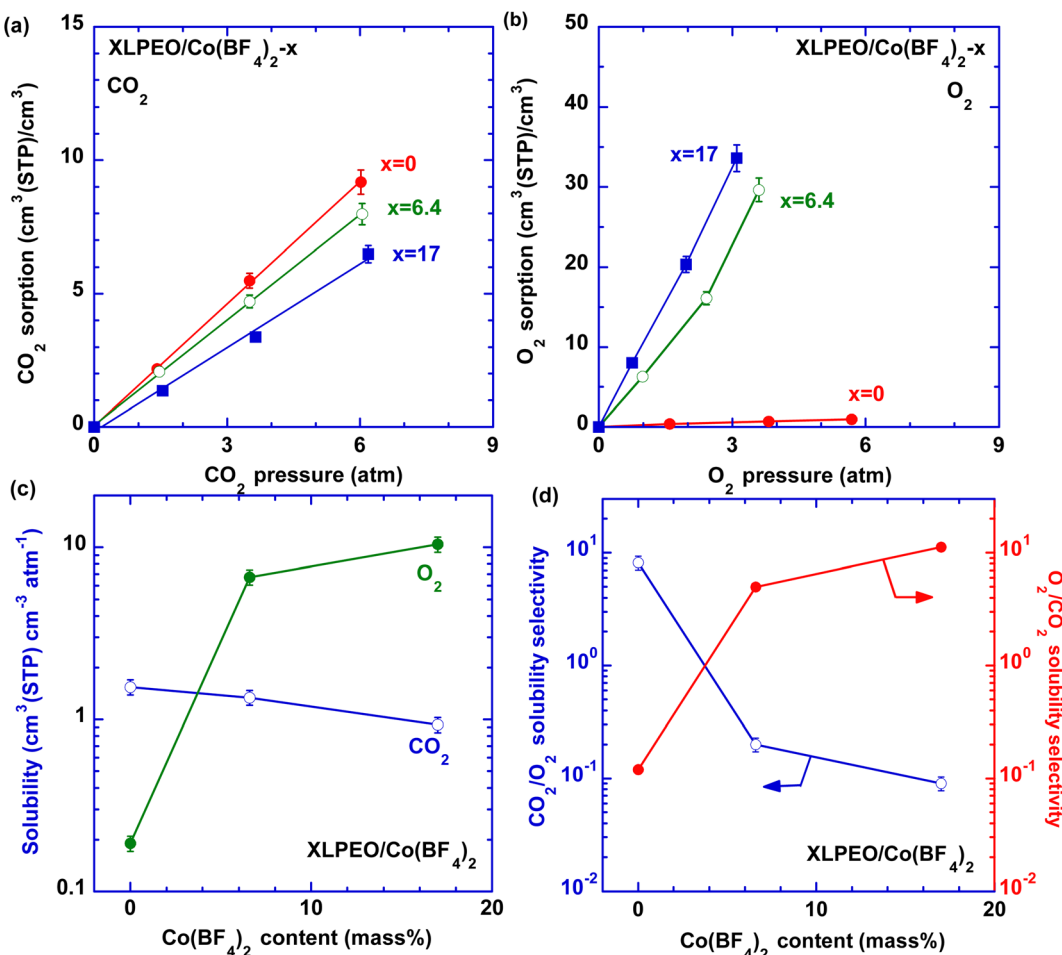


Fig. 3 Enormous O₂ sorption in XLPEO/Co(BF₄)₂ SPNs at 35 °C. Effect of the Co(BF₄)₂ loading on (a) CO₂ sorption isotherms, (b) O₂ sorption isotherms, (c) CO₂ and O₂ solubility, and (d) CO₂/O₂ solubility selectivity.

Fig. 2b and S1b† show that both series of SPNs are amorphous at ≈ 23 °C, validating complete dissociation of the Co salts by XLPEO. Adding salts has a minimal effect on the *d*-spacing (4.2 Å). Fig. 2c shows that increasing salt content increases ρ_{SP} (Tables 2 and S2†), which can be described using an additive model:³¹

$$\frac{1}{\rho_{SP}} = \frac{w_P}{\rho_P} + \frac{w_S}{\rho_S} = \frac{1}{\rho_P} + \left(\frac{1}{\rho_S} - \frac{1}{\rho_P} \right) w_S \quad (1)$$

where w is the mass fraction, and the subscripts of *P* and *S* represent properties of XLPEO and the amorphous salt, respectively. The fittings yield a ρ_S value of 3.84 g cm⁻³ for amorphous Co(ClO₄)₂ and 2.83 g cm⁻³ for amorphous Co(BF₄)₂. However, there are no reported values for anhydrous crystalline or dissociated amorphous Co(ClO₄)₂ or Co(BF₄)₂ in the literature for comparison.

Fig. S1c and d† present the DSC thermograms of the SPNs. All samples do not show degradation at the temperatures ranging from -90 to 100 °C, indicating their potential applications for typical O₂ purification (~ 23 °C). XLPEO shows a crystallization peak at -36 °C and a melting peak at -7 °C, which disappear after adding Co(BF₄)₂ because of the

complexation between ethylene oxides and Co²⁺. The absence of melting peaks at around 0 °C also suggests the absence of water in these films.³² Additionally, increasing salt loading increases $T_{g,SP}$ (Tables 2 and S2†), which can be described using an empirical equation:^{26,33}

$$1/T_{g,SP} = 1/T_{g,P} - ac_S \quad (2)$$

where $T_{g,P}$ is the glass transition temperature of XLPEO (K), a is an adjustable constant, and c_S is Co²⁺ content (kmol m⁻³). Fig. 2d shows that the best fit yields a value of 8.1×10^{-4} m³ kmol⁻¹ K⁻¹, close to that for XLPEO/Ni(BF₄)₂ (9.3×10^{-4} m³ kmol⁻¹ K⁻¹, Table S2†).²⁶

Gas sorption properties of SPNs

To elucidate the effect of the salt content on gas transport properties, CO₂ and O₂ sorption isotherms for XLPEO/Co(BF₄)₂ were obtained at 35 °C and are displayed in Fig. 3a and b. CO₂ and O₂ solubility can be calculated (Fig. 3c and Table S3†). Increasing Co(BF₄)₂ loading decreases CO₂ solubility and significantly increases O₂ solubility. For instance, adding 6.4 mass% Co(BF₄)₂ in XLPEO increases O₂ solubility from 0.19 to

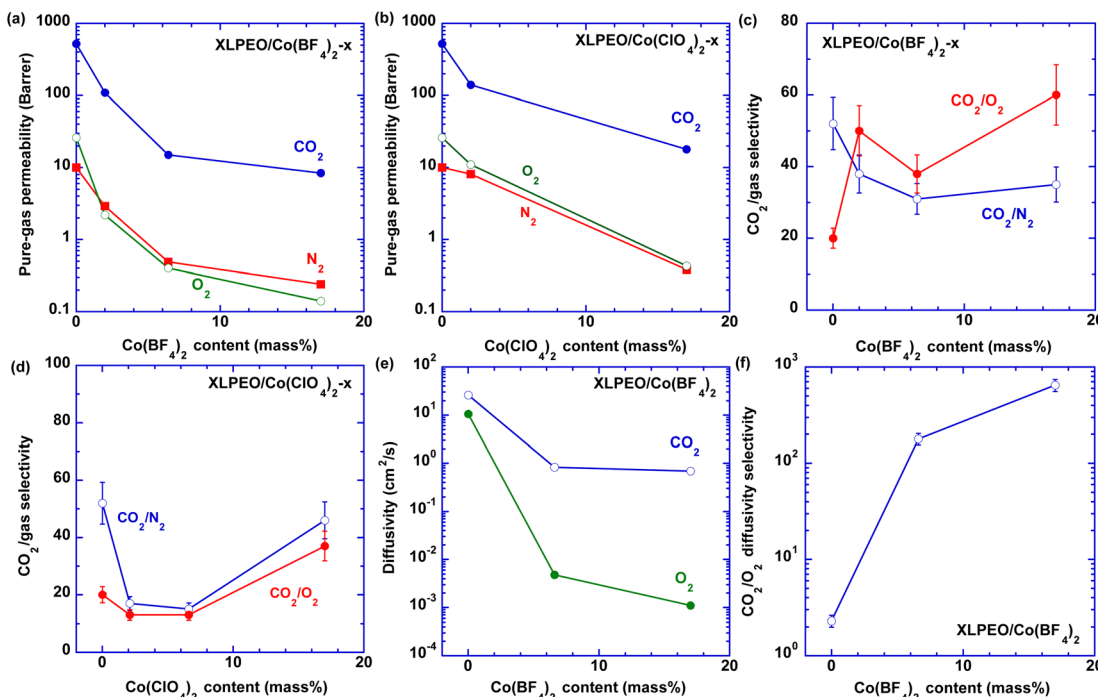


Fig. 4 Pure-gas transport properties of the SPNs at 35 °C. Dependence of gas permeability on (a) $\text{Co}(\text{BF}_4)_2$ loading and (b) $\text{Co}(\text{ClO}_4)_2$ loading. Dependence of CO_2 /gas selectivity on (c) $\text{Co}(\text{BF}_4)_2$ loading and (d) $\text{Co}(\text{ClO}_4)_2$ loading. Effect of the $\text{Co}(\text{BF}_4)_2$ loading on (e) CO_2 and O_2 diffusivity and (f) CO_2/O_2 diffusivity selectivity.

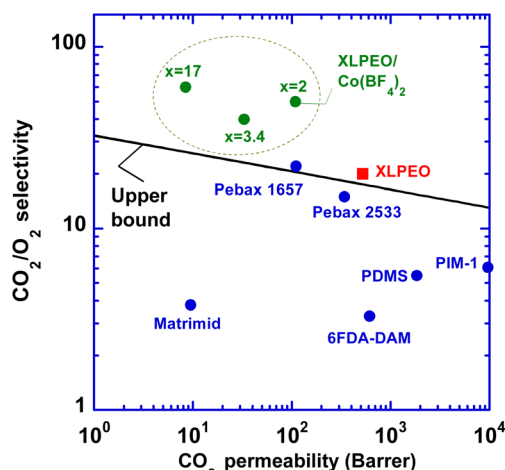


Fig. 5 Superior CO_2/O_2 separation properties in $\text{XLPEO}/\text{Co}(\text{BF}_4)_2$ ($x = 2, 3.4$, and 17) compared with Robeson's upper bound,^{36,37} and representative polymers, including Matrimid,⁶ Pebax 1657 and 2533,⁹ 6FDA-DAM,³⁸ PDMS,¹ and PIM-1.³⁹

6.7 $\text{cm}^3(\text{STP}) \text{cm}^{-3} \text{atm}^{-1}$ because of the Co^{2+} - O_2 complexation and decreases CO_2 solubility from 1.5 to 1.3 $\text{cm}^3(\text{STP}) \text{cm}^{-3} \text{atm}^{-1}$ due to the competitive interactions with XLPEO from the Co^{2+} ions. More importantly, increasing the $\text{Co}(\text{BF}_4)_2$ content decreases CO_2/O_2 solubility selectivity and significantly increases O_2/CO_2 solubility selectivity (Fig. 3d and e). In contrast, adding $\text{Co}(\text{ClO}_4)_2$ has minimal impact on O_2 solubility (Fig. S2a†). Although the underlying mechanism for missing O_2

affinity in $\text{XLPEO}/\text{Co}(\text{ClO}_4)_2$ is unclear, it is widely reported that anions and ligands can significantly influence the complexation between Co^{2+} and O_2 . For example, Co^{2+} -based carriers with different anions exhibited a wide range of O_2 sorption values between 0.06 and 0.90 mol O_2 per mol carrier at 16 cm_{Hg} .¹¹ Similarly, when various silver salts were dissolved in PEO for C_3H_6 sorption, the SPNs showed a molar ratio of C_3H_6 to Ag^+ of 0.49 for AgBF_4 , 0.13 for AgCF_3SO_3 , but only 0.03 for AgNO_3 ;³⁴ anions of bis(trifluoromethylsulfonyl)imide (Tf_2N^-) stabilized Ag^+ against H_2 , but not NO_3^{2-} anions.³⁵

Gas permeation properties of the SPNs

Fig. 4a and b present the effect of the $\text{Co}(\text{BF}_4)_2$ and $\text{Co}(\text{ClO}_4)_2$ content in XLPEO on pure-gas permeability at 35 °C (a typical temperature used for membrane applications), respectively. Increasing the salt loading decreases gas permeability because of the increased $T_{g,\text{SP}}$. For instance, adding 17 mass% $\text{Co}(\text{BF}_4)_2$ decreases CO_2 permeability by 98.4% from 520 to 8.4 barrer and O_2 permeability by 99.5% from 26 to 0.14 barrer. Similar behaviors have been observed for XLPEO with the addition of LiClO_4 , $\text{Ni}(\text{BF}_4)_2$, and $\text{Cu}(\text{BF}_4)_2$ were correlated with the increased $T_{g,\text{SP}}$.²⁶ Increasing the salt content also decreases CO_2/N_2 selectivity because of the interactions between Co^{2+} and XLPEO, which reduce the favorable interactions between CO_2 and XLPEO. Importantly, $\text{XLPEO}/\text{Co}(\text{BF}_4)_2$ SPNs exhibit unexpected CO_2/O_2 selectivity. For instance, adding only 3.4 mass% $\text{Co}(\text{BF}_4)_2$ increases CO_2/O_2 selectivity from 20 to 40, while adding $\text{Co}(\text{ClO}_4)_2$ consistently decreases CO_2/O_2 selectivity (Table S1†). Interestingly, $\text{XLPEO}/\text{Co}(\text{BF}_4)_2$ SPNs even show O_2/N_2

selectivity less than 1 (Fig. S2b†), which is very unusual for polymeric films.

CO_2 and O_2 diffusion coefficients ($D_A, \text{ cm}^2 \text{ s}^{-1}$) can be calculated by using $D_A = P_A/S_A$, and the results are shown in Fig. 4e, f, S2c and Table S3.† Increasing the Co salt content decreases CO_2 diffusivity because of the decreased chain flexibility, as indicated by the increased $T_{g,\text{SP}}$. Importantly, adding 17 mass% $\text{Co}(\text{BF}_4)_2$ increases CO_2/O_2 diffusivity selectivity from 2.3 to 650, validating the retarded O_2 diffusion in the XLPEO/ $\text{Co}(\text{BF}_4)_2$ SPNs. In contrast, adding 17 mass% $\text{Co}(\text{ClO}_4)_2$ increases CO_2/O_2 diffusivity selectivity only to 5.7 (Fig. S2c†).

CO₂/O₂ separation properties

Fig. 5 exhibits superior CO_2/O_2 separation properties of the XLPEO/ $\text{Co}(\text{BF}_4)_2$ SPNs in Robeson's upper bound plot.^{36,37} All XLPEO/ $\text{Co}(\text{BF}_4)_2$ SPNs ($x = 2, 3.4$, and 17) exhibit CO_2/O_2 separation properties above the upper bound.

Our preliminary data show that the SPNs may lose separation properties over time, as shown in Table S4.† After storage in a vacuum for ~ 4 months, a freestanding film (XLPEO/ $\text{Co}(\text{BF}_4)_2$ -5) was tested with CO_2 at 50 psig and O_2 at 100 psig alternatively for 9 days. CO_2 permeability decreased from 75 to 12 barrer, and CO_2/O_2 selectivity decreased from 100 to 48, presumably because of the instability of Co^{2+} ions. Though CO_2/O_2 selectivity is still above the upper bound, the practical applications of these SPNs will need more investigation.

Conclusion

We began this work with a hypothesis that Co^{2+} -based carriers can be incorporated into XLPEO to increase O_2 sorption and permeability because of the affinity of O_2 towards Co^{2+} . $\text{Co}(\text{BF}_4)_2$ at loadings as high as 17 mass% can be dissociated by XLPEO to form SPNs, as indicated by DSC and XRD results. As expected, increasing $\text{Co}(\text{BF}_4)_2$ content increases $T_{g,\text{SP}}$ and density and decreases gas permeability. Importantly, it dramatically increases O_2 solubility and O_2/CO_2 solubility selectivity. Surprisingly, the XLPEO/ $\text{Co}(\text{BF}_4)_2$ SPNs exhibit extremely low O_2 permeability due to the retarded O_2 diffusion and thus unexpectedly high CO_2/O_2 permeability selectivity, surpassing Robeson's upper bound and current leading materials for CO_2/O_2 separation. This study unveils a new series of SPNs with the potential for CO_2/O_2 separations, and the discovered retarded diffusion may be harnessed to design high-performance materials for various gas and vapor separations.

Interestingly, adding $\text{Co}(\text{ClO}_4)_2$ into XLPEO does not improve O_2 sorption and decreases CO_2/O_2 permeability selectivity. We expect that the anion type influences the dissociation of the Co salts and the ability of Co^{2+} ions to interact with polymers and O_2 . Additionally, Co^{2+} is subjected to oxidation and converted to Co^{3+} without affinity towards O_2 . Therefore, experimental investigation and computational simulations will be needed to unravel the underlying mechanisms and determine the carrier stability. Future work should also focus on preparing thin-film composite membranes and evaluating them with real gas streams to determine long-term stability.

Author contributions

T. A.: conceptualization, investigation, data curation, writing – original draft preparation; N. E.: data curation and discussion, writing-reviewing and editing; G. Z.: data curation and discussion, writing-reviewing and editing; H. L.: conceptualization, writing-reviewing and editing, supervision.

Conflicts of interest

There are no conflicts to declare.

Acknowledgements

This work received financial support from the U.S. Department of Energy Small Business Technology Transfer Program (DE-SC0020730), the National Energy Technology Laboratory (DE-FE0031736), and the New York State Foundation for Science, Technology and Innovation (NYSTAR).

References

- 1 J. Wang, F. Kang, Y. Chen, X. Zhang, X. Jiang, G. He and X. Ruan, *Sep. Purif. Technol.*, 2024, **337**, 126461.
- 2 Z. Zhao, W. Gao, Y. Chang, Y. Yang, H. Shen, T. Li and S. Zhao, *Adv. Healthcare Mater.*, 2023, **690**, 122183.
- 3 B. S. Kirkland, R. Clarke and D. R. Paul, *J. Membr. Sci.*, 2008, **324**, 119–127.
- 4 T. C. Merkel, X. Wei, Z. He, L. S. White, J. G. Wijmans and R. W. Baker, *Ind. Eng. Chem. Res.*, 2013, **52**, 1150–1159.
- 5 J. Wu, F. Hillman, C.-Z. Liang, Y. Jia and S. Zhang, *J. Mater. Chem. A*, 2023, **11**, 17452–17478.
- 6 T.-S. Chung, S. S. Chan, R. Wang, Z. Lu and C. He, *J. Membr. Sci.*, 2003, **211**, 91–99.
- 7 B. Zhu, X. Jiang, S. He, X. Yang, J. Long, Y. Zhang and L. Shao, *J. Mater. Chem. A*, 2020, **8**, 24233–24252.
- 8 H. Lin and B. D. Freeman, *J. Membr. Sci.*, 2004, **239**, 105–117.
- 9 V. I. Bondar, B. D. Freeman and I. Pinna, *J. Polym. Sci., Part B: Polym. Phys.*, 2000, **38**, 2051–2062.
- 10 X. Chen, H. Nishide, K. Oyaizu and E. Tsuchida, *J. Phys. Chem. B*, 1997, **101**, 5725–5729.
- 11 B. M. Johnson, R. W. Baker, S. L. Matson, K. L. Smith, I. C. Roman, M. E. Tuttle and H. K. Lonsdale, *J. Membr. Sci.*, 1987, **31**, 31–67.
- 12 Y. Kohno, M. G. Cowan, A. Okafuji, H. Ohno, D. L. Gin and R. D. Noble, *Ind. Eng. Chem. Res.*, 2015, **54**, 12214–12216.
- 13 H. Zhao, T. Song, X. Ding, R. Cai, X. Tan and Y. Zhang, *J. Membr. Sci.*, 2023, **679**, 121713.
- 14 D. E. Jaramillo, A. Jaffe, B. E. Snyder, A. Smith, E. Taw, R. C. Rohde, M. N. Dods, W. DeSnoo, K. R. Meihaus and T. D. Harris, *Chem. Sci.*, 2022, **13**, 10216–10237.
- 15 H. Nishide, H. Kawakami, S. Toda, E. Tsuchida and Y. Kamiya, *Macromolecules*, 1991, **24**, 5851–5855.
- 16 H. Nagar, P. Vadthya, N. S. Prasad and S. Sridhar, *RSC Adv.*, 2015, **5**, 76190–76201.
- 17 S. H. Chen and J. Y. Lai, *J. Appl. Polym. Sci.*, 1996, **59**, 1129–1135.



- 18 W. Choi, P. G. Ingole, H. Li, S. Y. Park, J. H. Kim, H.-K. Lee and I.-H. Baek, *Microchem. J.*, 2017, **132**, 36–42.
- 19 J. Han, L. Bai, S. Luo, B. Yang, Y. Bai, S. Zeng and X. Zhang, *Sep. Purif. Technol.*, 2020, **248**, 117041.
- 20 E. Khare, N. Holten-Andersen and M. J. Buehler, *Nat. Rev. Mater.*, 2021, **6**, 421–436.
- 21 L. Hu, V. T. Bui, S. Fan, W. Guo, S. Pal, Y. Ding and H. Lin, *J. Mater. Chem. A*, 2022, **10**, 10872–10879.
- 22 Y. Fu, L. Chen, F. Xu, X. Li, Y. Li and J. Sun, *J. Mater. Chem. A*, 2022, **10**, 4695–4702.
- 23 A. Morisato, Z. J. He, I. Pinna and T. C. Merkel, *Desalination*, 2002, **145**, 347–351.
- 24 T. C. Merkel, R. Blanc, I. Ciobanu, B. Firat, A. Suwarlim and J. Zeid, *J. Membr. Sci.*, 2013, **447**, 177–189.
- 25 H. Lin, E. Van Wagner, J. S. Swinnea, B. D. Freeman, S. J. Pas, A. J. Hill, S. Kalakkunnath and D. S. Kalika, *J. Membr. Sci.*, 2006, **276**, 145–161.
- 26 T. Alebrahim, A. Chakraborty, L. Hu, S. Patil, S. Cheng, D. Acharya, C. M. Doherty, A. J. Hill, T. R. Cook and H. Lin, *J. Membr. Sci.*, 2022, **644**, 120063.
- 27 T. Alebrahim, L. Huang, H. K. Welgama, N. Esmaeili, E. Deng, S. Cheng, D. Acharya, C. M. Doherty, A. J. Hill, C. Rumsey, M. Trebbin, T. R. Cook and H. Lin, *ACS Appl. Mater. Interfaces*, 2024, **16**, 11116–111124.
- 28 K. M. Rodriguez, W. Wu, T. Alebrahim, Y. Cao, B. D. Freeman, D. Harrigan, M. Jhalaria, A. Kratochvil, S. Kumar, W. Lee, Y. Lee, H. Lin, J. M. Richardson, Q. Song, B. Sundell, R. Thur, I. Vankelecom, A. Wang, C. Wiscount, J. Xingming and Z. P. Smith, *J. Membr. Sci.*, 2022, **659**, 120746.
- 29 P. R. Bevington and D. K. Robinson, *Data reduction and error analysis for the physical sciences*, McGraw-Hill, Inc., New York, 2nd edn, 1992.
- 30 T. Tran, Y. Fu, D. Jiang and H. Lin, *Macromolecules*, 2022, **55**, 9860–9867.
- 31 N. Paranjape, P. C. Mandadapu, G. Wu and H. Lin, *Polymer*, 2017, **111**, 1–8.
- 32 T. Tran, C. Lin, S. Chaurasia and H. Lin, *J. Membr. Sci.*, 2019, **574**, 299–308.
- 33 C. J. Hawker, F. K. Chu, P. J. Pomery and D. J. T. Hill, *Macromolecules*, 1996, **29**, 3831–3838.
- 34 S. Sunderrajan, B. D. Freeman, C. K. Hall and I. Pinna, *J. Membr. Sci.*, 2001, **182**, 1–12.
- 35 S. Park, O. Morales-Collazo, B. Freeman and J. F. Brennecke, *Angew. Chem., Int. Ed.*, 2022, **61**, e202202895.
- 36 B. D. Freeman, *Macromolecules*, 1999, **32**, 375–380.
- 37 H. Lin and M. Yavari, *J. Membr. Sci.*, 2015, **475**, 101–109.
- 38 L. Shao, T.-S. Chung, S. H. Goh and K. P. Pramoda, *J. Membr. Sci.*, 2005, **267**, 78–89.
- 39 C. G. Bezzu, A. Fuoco, E. Esposito, M. Monteleone, M. Longo, J. C. Jansen, G. S. Nichol and N. B. McKeown, *Adv. Funct. Mater.*, 2021, **31**, 2104474.

